inorganics

MDPI

Article

3-Methylindole-Based Tripodal Tetraphosphine Ruthenium Complexes in N_2 Coordination and Reduction and Formic Acid Dehydrogenation

Fenna F. van de Watering, Nicol Heijtbrink, Jarl Ivar van der Vlugt, Wojciech I. Dzik, Bas de Bruin * and Joost N. H. Reek *

Homogeneous, Supramolecular and Bio-Inspired Catalysis Group, Van't Hoff Institute for Molecular Sciences, University of Amsterdam, Science Park 904, 1098 XH Amsterdam, The Netherlands; fenna@van-de-watering.nl (F.F.v.d.W.); nicolheijtbrink@hotmail.com (N.H.); J.I.vanderVlugt@uva.nl (J.I.v.d.V.); wdzik@wp.pl (W.I.D.)

* Correspondence: B.deBruin@uva.nl (B.d.B); J.N.H.Reek@uva.nl (J.N.H.R.); Tel.: +31-020-525-6495 (B.d.B); +31-020-5256437 (J.N.H.R.)

Received: 27 September 2017; Accepted: 25 October 2017; Published: 30 October 2017

Abstract: The ruthenium(II) complexes $RuCl_2$**L1**^{H}, $RuCl_2$**L1**^{CF3}, $RuCl_2$**L1**^{OMe} and $RuCl_2$**L2**^{H} were synthesized from $[Ru(\eta^6\text{-benzene})Cl(\mu\text{-}Cl)]_2$ and the corresponding tripodal tris-3-methylindolephosphine-based ligands **L1**^{H}, **L1**^{CF3}, **L1**^{OMe}, and **L2**^{H}. Stoichiometric reduction of these complexes with KC_8 yielded the corresponding ruthenium(0) dinitrogen complexes. The latter complexes were studied in the N_2 reduction with chlorosilanes and KC_8, yielding stoichiometric amounts of the silylamines. The synthesized ruthenium(II) complexes are also active catalysts for the formic acid dehydrogenation reaction.

Keywords: ruthenium; N_2 activation; formic acid dehydrogenation; tripodal tetraphosphine ligands

1. Introduction

Electrocatalytic reduction reactions that store energy by the conversion of H^+, CO_2, or N_2, are important in the context of the transformation to a society based on sustainable energy. Therefore, the development of efficient catalysts that enable these reactions is needed. Homogeneous tripodal ligand transition metal complexes have shown beneficial reactivity over mono- or bidentate ligands in many organic transformations [1–3]. In recent years, tripodal ligands coordinated to molybdenum, iron, and cobalt were shown to lead to complexes that are capable of the reduction of N_2 to ammonia or silylamines [4–10]. Also, reversible hydrogen storage in CO_2 was shown to be possible with iron and cobalt based on tripodal ligands [11–13]. Previously, we reported the coordination of ligand **L1**^{H} (Figure 1) to rhodium [14,15] and ruthenium [16]. This ligand, which features three 1-(3-methylindolyl)diphenylphosphine groups tethered to a central phosphorus atom, stabilizes ruthenium in the oxidation states +II, +I, and 0. The isolated low oxidation state $Ru^{I}Cl$**L1**^{H} and $Ru^{0}(N_2)$**L1**^{H} complexes revealed interesting one-electron reactivity, as they were able to abstract chlorine atoms from either chloroform or dichloromethane, leading to formation of the corresponding Ru^{II} complex. In this paper, we expand the coordination chemistry of ruthenium and 3-methylindole-based ligands [17–23] and investigate how modification of the ligand scaffold and its electronic properties influence the stability and activity of these complexes in dinitrogen coordination and subsequent reduction as well as in formic acid dehydrogenation. Ligand **L1**^{H} was modified using functionalized $P(Ar)_2$ units, wherein the arene carries either electron-withdrawing $-CF_3$ groups (**L1**^{CF3}) or electron-donating –OMe groups (**L1**^{OMe}) in the *para*-position (Figure 1). Additionally, the known

structural isomer, $\mathbf{L2^H}$ (Figure 2) [14], in which the central P-donor is bound to the three nitrogen atoms of the 2-(3-methylindolyl)diphenylphosphine moiety, was also used in these studies.

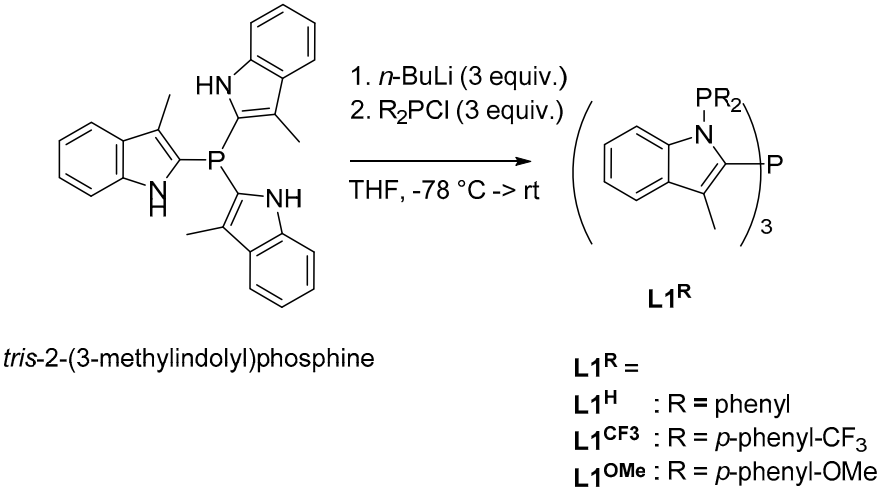

Figure 1. Synthesis of ligands $\mathbf{L1^R}$ by reacting tris-2-(3-methylindolyl)phosphine with the corresponding chlorodiarylphosphine.

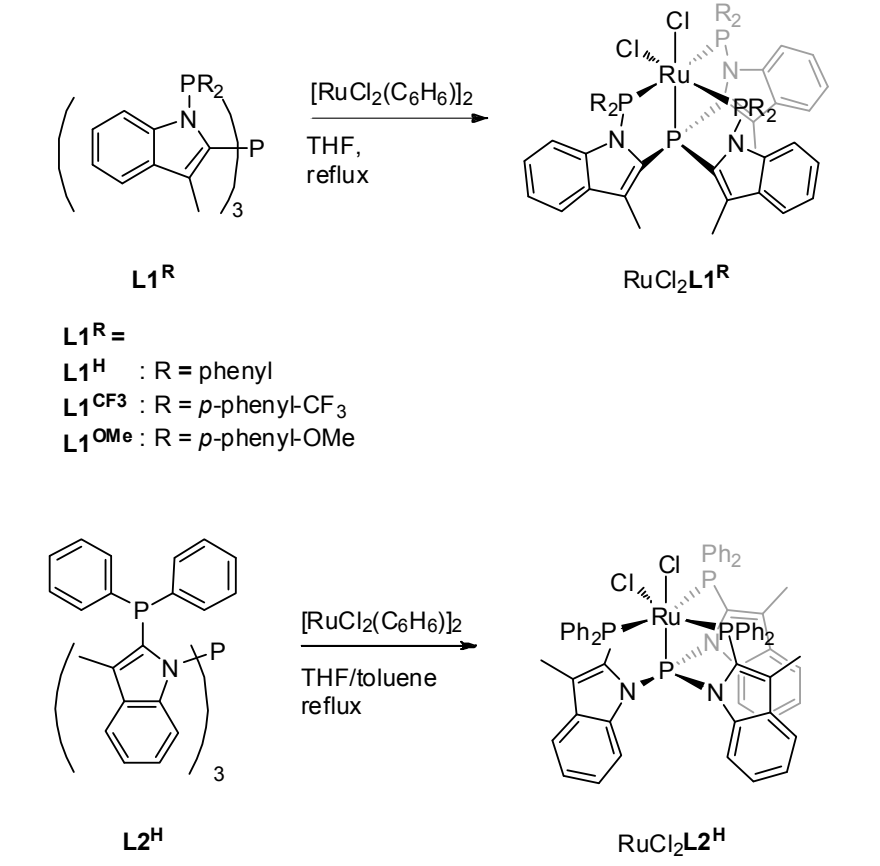

Figure 2. Ruthenium complexes of $\mathbf{L1^R}$ and $\mathbf{L2^H}$.

2. Results

Ligands $\mathbf{L1^H}$ and $\mathbf{L2^H}$ were prepared in two steps from 3-methylindole as previously reported by our group [14,15]. The new ligands $\mathbf{L1^{CF3}}$ and $\mathbf{L1^{OMe}}$ were prepared in a similar way to $\mathbf{L1^H}$,

by reacting tris-2-(3-methylindolyl)phosphine [17] with the corresponding chlorodiarylphosphine (Figure 1).

The reaction of $\mathbf{L1^H}$ with [Ru(η^6-benzene)Cl(μ-Cl)]$_2$ in refluxing THF for 16 h led to the formation of the octahedral complex $RuCl_2\mathbf{L1^H}$ in quantitative yield (Figure 2). Surprisingly, the other ligands did not react with this ruthenium precursor in refluxing THF. Even after 36 h, only trace amounts of the target complexes were observed using ex-situ ^{31}P NMR spectroscopy, and mainly signals of the unreacted ligand were present. Reactions in refluxing THF/toluene (1:3) mixture at 120 °C for a prolonged time of 64 h did lead to the formation of complexes $RuCl_2\mathbf{L1^{CF3}}$, $RuCl_2\mathbf{L1^{OMe}}$, and $RuCl_2\mathbf{L2^H}$ in >50% isolated yields.

All three **L1**-based $RuCl_2\mathbf{L1}$ complexes show similar ^{31}P NMR spectra: three signals in a ratio 1(td):2(t):1(td) (Figure 3). This splitting pattern indicates the formation of a symmetric complex. Ruthenium(II) complexes tend to form octahedral 18-valence electron complexes, and X-ray analysis and NMR spectroscopy confirmed that complex $RuCl_2\mathbf{L1^H}$ indeed features an octahedral geometry with the two chlorides in mutual *cis* position and all four phosphines bound to the metal center [15]. The above factors and the similarity of the ^{31}P NMR spectra of the other **L1**-based complexes point to the same octahedral geometry around the metal center.

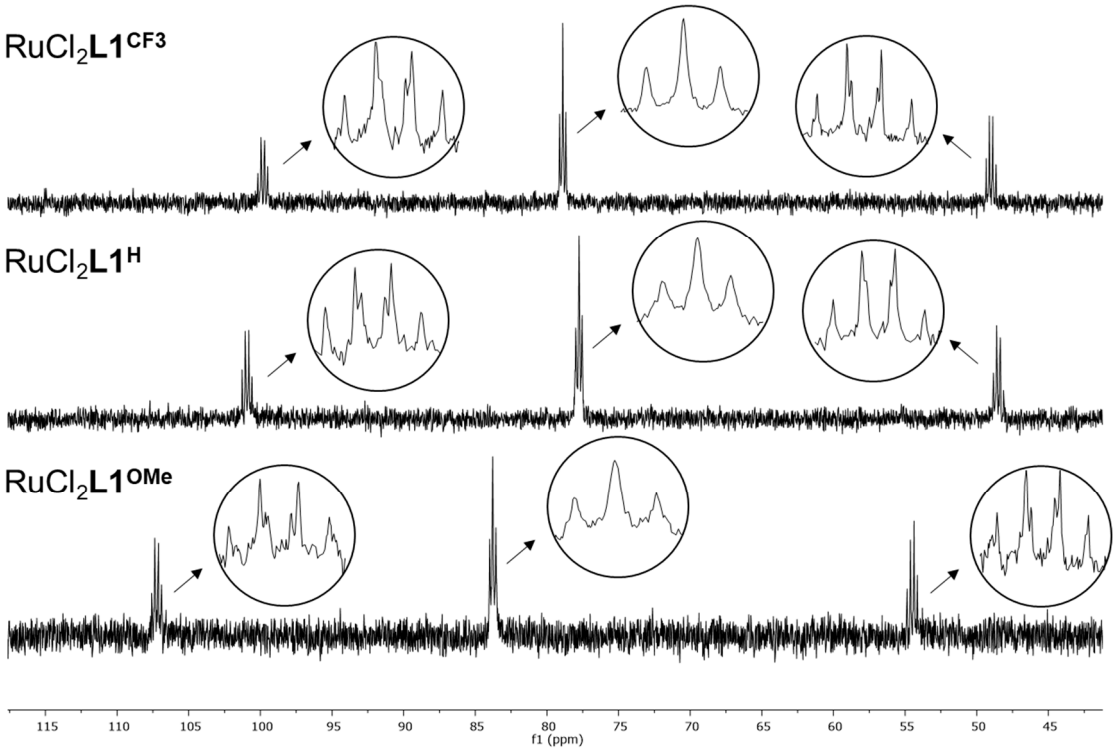

Figure 3. ^{31}P-NMR spectra of $\mathbf{L1^R}$-based ruthenium(II) dichlorido complexes.

Layering of a dichloromethane solution of $RuCl_2\mathbf{L1^{CF3}}$ with pentane resulted in the formation of crystals suitable for single-crystal X-ray diffraction. The crystal structure (Figure 4) of $RuCl_2\mathbf{L1^{CF3}}$ indeed shows an overall octahedral geometry with the chlorido ligands in *cis* position, in accordance with the observed ^{31}P NMR splitting pattern. The P1–Ru–P2 angle in $RuCl_2\mathbf{L1^{CF3}}$ (157.78(6)°) is comparable to the one previously reported for $RuCl_2\mathbf{L1^H}$ (160.04(3)°) (Table 1). The P1–Ru, P2–Ru and P3–Ru bond lengths are all slightly smaller in $RuCl_2\mathbf{L1^{CF3}}$ (2.3097(19) Å, 2.3445(19) Å and 2.2383(17) Å, respectively) compared with $RuCl_2\mathbf{L1^H}$ (2.3189(9) Å, 2.3727(9) Å and 2.2671(9) Å). The –CF_3 groups clearly point away from the metal center, so steric effects do not play a significant role in the coordination chemistry. The C_s symmetry observed in solution by ^{31}P NMR spectroscopy for both $RuCl_2\mathbf{L1^H}$ and $RuCl_2\mathbf{L1^{CF3}}$ is not present in the solid state, as the unit cell contains two rotamers.

This becomes evident when the symmetry-equivalent molecules in the crystal structure of $RuCl_2$**L1**^{CF3} are viewed from the bottom: the indolyl moieties either all point clockwise, or counter-clockwise (Figure 5, showing the bottom view of $RuCl_2$**L1**^{CF3} and a schematic representation). In solution, these two rotamers seem to rapidly interchange on the NMR timescale, resulting in one signal for the two mutually *trans* phosphines. Likely, the methyl groups of the indolyl moiety do not create enough steric repulsion to suppress this process. Despite several attempts, no crystals suitable for X-ray diffraction of the $RuCl_2$**L1**^{OMe} complex were obtained.

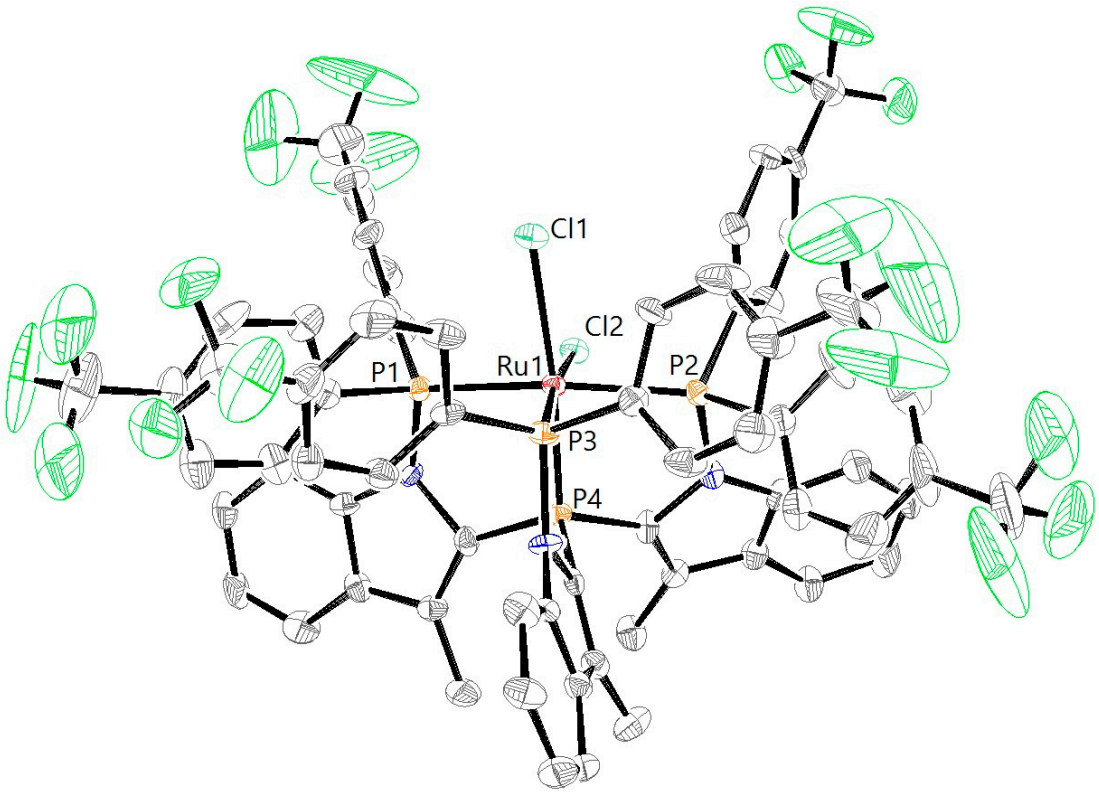

Figure 4. ORTEP drawing of $RuCl_2$**L1**^{CF3} (CCDC 1574141) showing one of the two rotamers. Thermal ellipsoids are set at 50% probability. Solvent molecules and hydrogen atoms have been omitted for clarity.

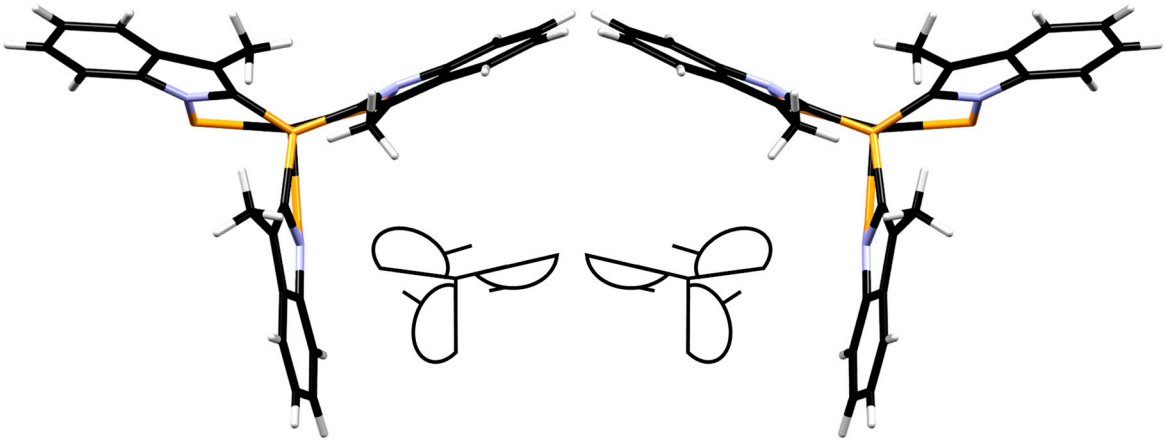

Figure 5. Drawing of bottom view of $RuCl_2$**L1**^{CF3} of both isomers, showing only the (3-methylindolyl)phosphine part. Insert: schematic representation of the two rotamers with the 3-methylindolyl moiety twisted clockwise (**left**) or counter-clockwise (**right**).

Table 1. Selected bond lengths (Å) and angles (°) for Ru**L** complexes.

	$RuCl_2L1^{H}$ [a]	$RuCl_2L1^{CF3}$	$RuCl_2L2^{H}$	$RuN_2L_1^{H}$	RuN_2L1^{CF3}
Ru1–P1	2.3189(9)	2.3097(19)	2.3295(8)	2.2747(12)	2.2613(10)
Ru1–P2	2.3727(9)	2.3445(19)	2.4079(8)	2.2752(11)	2.2702(10)
Ru1–P3	2.2671(9)	2.2383(17)	2.2913(8)	2.2774(11)	2.2554(10)
Ru1–P4	2.1932(9)	2.2023(17)	2.1363(8)	2.2133(11)	2.2193(9)
Ru1–Cl1	2.4869(9)	2.4869(16)	2.4829(7)		
Ru1–Cl2	2.4471(9)	2.4487(16)	2.4705(7)		
Ru1–N1				2.011(4)	2.066(3)
N1–N2				1.085(5)	1.064(5)
P1–Ru1–P2	160.04(3)	157.78(6)	159.24(3)	122.85(4)	119.79(4)
P1–Ru1–P3	102.23(3)	101.39(7)	101.30(3)	115.80(4)	119.28(4)
P2–Ru1–P3	94.27(3)	97.42(7)	93.60(3)	118.33(4)	118.16(4)
P1–Ru1–P4	87.06(3)	86.13(6)	86.13(3)	84.14(4)	84.54(4)
P2–Ru1–P4	82.67(3)	83.12(6)	80.63(3)	83.91(4)	84.13(4)
P3–Ru1–P4	86.85(3)	87.02(6)	85.62(3)	84.63(4)	84.73(3)

[a] Taken from reference [16].

Interestingly, complex $RuCl_2$**L2**^{H}, which is based on the linkage isomer of **L1**^{H}, ligand **L2**^{H}, displays a different ^{31}P NMR spectrum (Figure 6). The four signals, two triplets of doublets and two doublets of doublets of doublets with an AX pattern, each integrating one phosphine, indicate the formation of a complex with a different symmetry. Crystals obtained by layering of a DCM solution of $RuCl_2$**L2**^{H} with pentane at 5 °C were of sufficient quality for X-ray crystallography. The corresponding structure of complex $RuCl_2$**L2**^{H} (Figure 7) helps to understand the origin of the AX pattern, as the bottom view displays much more steric hindrance around the central phosphorus atom P4 (vide infra).

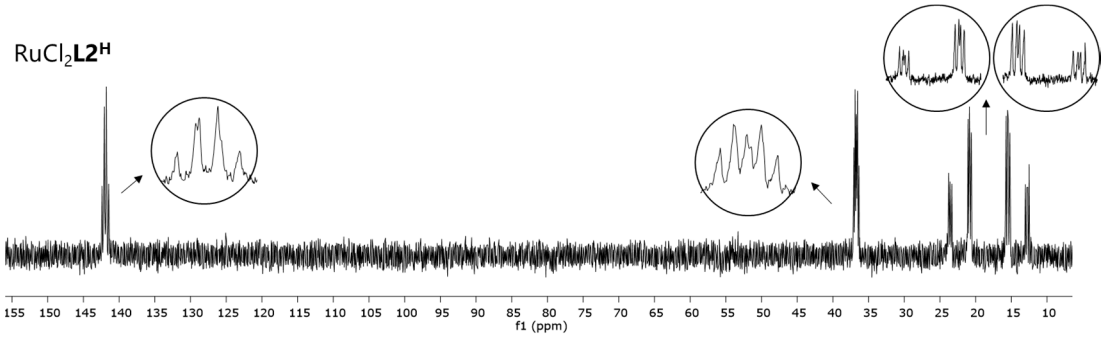

Figure 6. ^{31}P NMR spectrum of $RuCl_2$**L2**^{H}.

However, different than the **L1**-based complexes, where the methyl groups are pointing towards the central phosphine (Figure 5), in complex $RuCl_2$**L2**^{H}, the bulkier phenyl rings of the indolyl moiety point towards the central phosphine (Figure 8). From the crystal structure, it appears that these phenyl rings should encounter more hindrance toward inversion and it therefore seems likely that this process is associated with a high energy barrier in solution. As a result, the two phosphine atoms (P1 and P2, Figure 7) in *trans* position become inequivalent, leading to the observed AX pattern in the ^{31}P NMR spectrum as a result of the P1–P2 coupling.

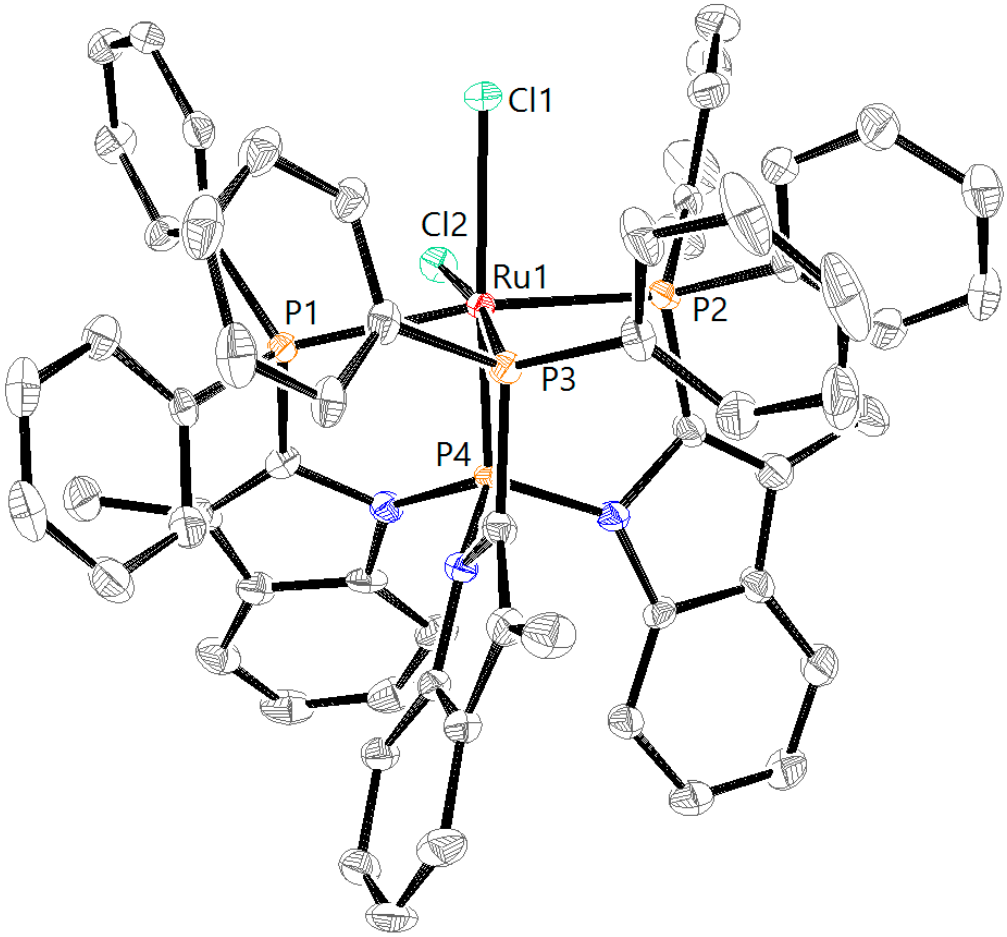

Figure 7. ORTEP drawing of $RuCl_2$**L2**^{H} (CCDC 1574140) showing a side view of one of the two rotamers. Thermal ellipsoids are set at 50% probability. Solvent molecules and hydrogen atoms have been omitted for clarity.

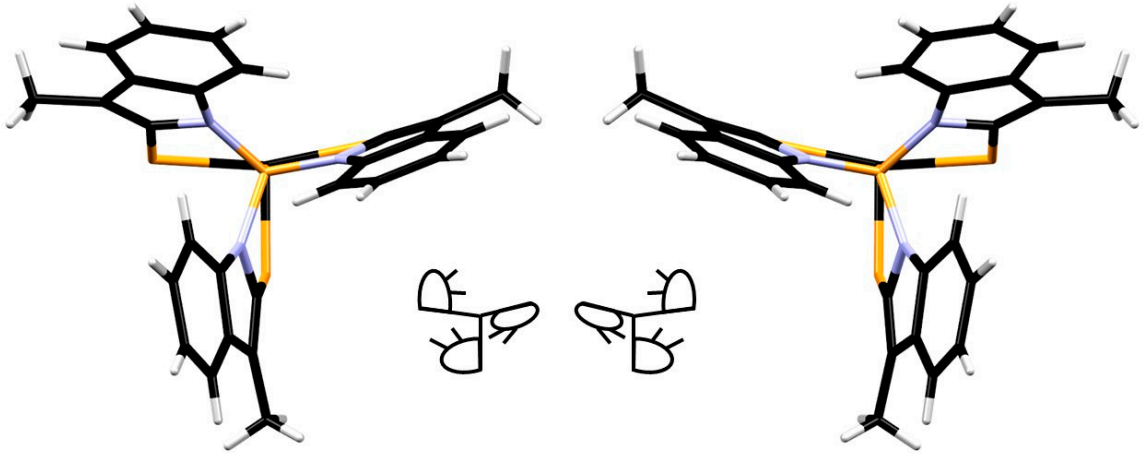

Figure 8. Bottom view of X-ray structure of $RuCl_2$**L2**^{H} of both rotamers, showing only the (3-methylindolyl)phosphine part. Insert: schematic representation of the two rotamers where the 3-methylindolyl moiety is twisted clockwise (**left**) or counter-clockwise (**right**).

The crystal structure of $RuCl_2$**L2**^{H} further reveals minor differences in the coordination around the ruthenium center compared with $RuCl_2$**L1**^{H} (Table 1). The P1–Ru, P2–Ru, and P3–Ru bond lengths

become slightly larger (2.3295(8) Å, 2.4079(8) and 2.2913(8) Å), but the P4–Ru bond (2.1363(8) Å) shortens, which is in line with a more π-acidic character of the tris(amido)phosphine P4 atom.

Two-electron reduction of $RuCl_2$**L1**^{H} under an N_2 atmosphere led to the formation of the RuN_2**L1**^{H} complex, which features a characteristic infrared band corresponding to the coordinated N_2 at 2125 cm^{-1} (Table 2) [15]. To explore if the electronic properties of the ligands **L1**^{CF3}, **L1**^{OMe}, and **L2**^{H} have an influence on the binding of N_2 to Ru^0, the corresponding N_2 complexes were generated in situ by reacting the ruthenium(+II) complexes with two equivalents of KC_8 (Figure 9). The extent of activation of the N_2 bond was quantified by measuring the N≡N stretch frequency with infrared spectroscopy, as this is a direct measure for the ligand-dependent π-back-donation. Table 2 shows the N_2 stretch frequencies of the Ru^0N_2**L** complexes.

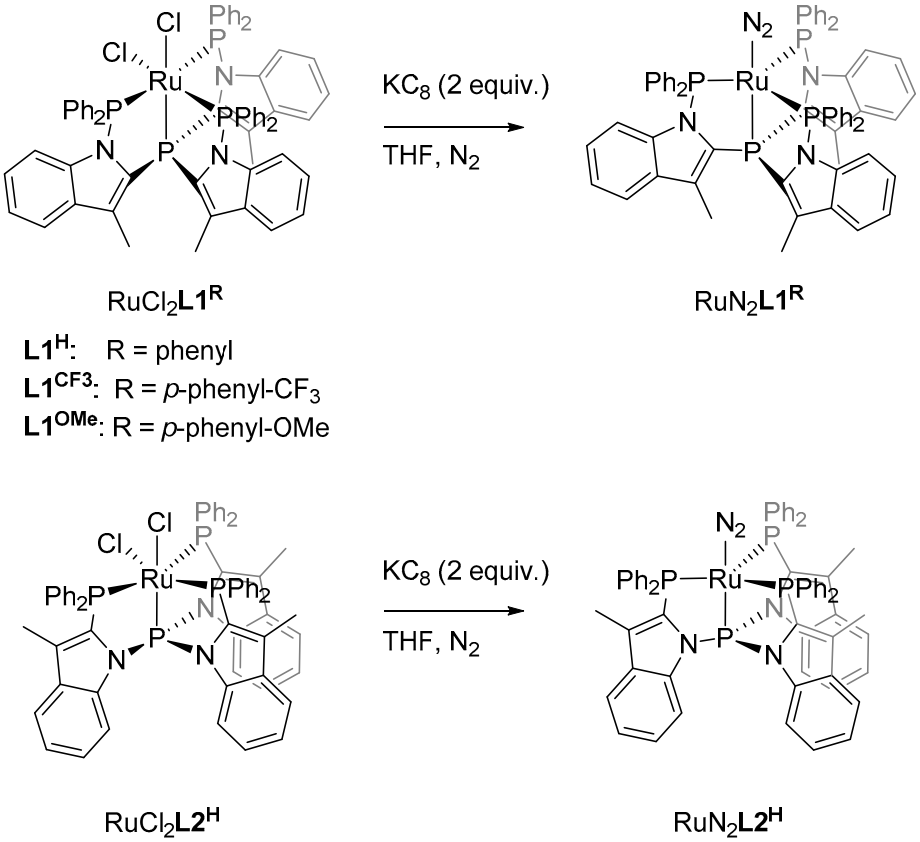

Figure 9. Reaction of $RuCl_2$**L** complexes with two equivalents of KC_8 in presence of N_2 forming the corresponding $Ru^0(N_2)$**L**.

Table 2. IR frequency of the selected $Ru^0(N_2)$**L** complexes.

Complex	ν_{N2} (cm^{-1})
RuN_2**L1**^{CF3}	2136
RuN_2**L1**^{H}	2125
RuN_2**L1**^{OMe}	2113
RuN_2**L2**^{H}	2136

As expected, the complex coordinated with the less electron-rich, CF_3 substituted ligand shows a band with a higher wavenumber in the infrared spectrum (2136 cm^{-1}), as a result of weaker metal-to-N_2 π-back-donation. The complex coordinated to the more electron-rich OMe substituted ligand shows a band at 2113 cm^{-1}, thus revealing stronger π-back-donation to N_2. Clearly, the peripheral phosphines induce measurable electronic effects on the *d*-orbitals of the ruthenium

center; the phosphines *cis* to the N_2 ligand become stronger σ-donors and weaker π-acceptors in $\mathbf{L1^{OMe}}$ and vice versa for $\mathbf{L1^{CF3}}$, which changes the binding properties of the N_2 ligand. Going from $RuN_2\mathbf{L1^H}$ (2125 cm^{-1}) to the structural isomer $RuN_2\mathbf{L2^H}$ (2136 cm^{-1}), the N_2 stretch frequency increases by 11 cm^{-1}. This is likely a result of the more π-acidic pivotal P-atom (atom P4, Figure 10, top) of the tris(amido)phosphine donor ligand, which competes with the N_2 ligand for π-back-donation from the same metal *d*-orbitals. Thus, substitution of the phosphine *trans* to the N_2 ligand for a more π-acidic group leads to weaker π-back-donation of Ru to N_2. These results show that the electronic properties of the dinitrogen complexes can be tuned by ligand design, either by manipulating the substitutions on the donor atoms coordinated *cis* to N_2 or by changing the π-acidity of the atom bound *trans* to N_2.

Layering of a THF solution of $RuN_2\mathbf{L1^{CF3}}$ with pentane resulted in the formation of single crystals suitable for X-ray diffraction (Figure 10). Similar to the $RuN_2\mathbf{L1^H}$ complex reported previously [15], $RuN_2\mathbf{L1^{CF3}}$ also shows a trigonal bipyramidal geometry. The N≡N bond is slightly shorter in $RuN_2\mathbf{L1^{CF3}}$ (1.064(5)°) than in $RuN_2\mathbf{L1^H}$ (1.085(5)°) (Table 1), which is in accordance with the observed trend in the activation of the N_2 stretch frequency (Table 2). In solution, these complexes remain trigonal bipyramidal, as judged from the occurrence of a doublet and a quartet in all ^{31}P NMR spectra.

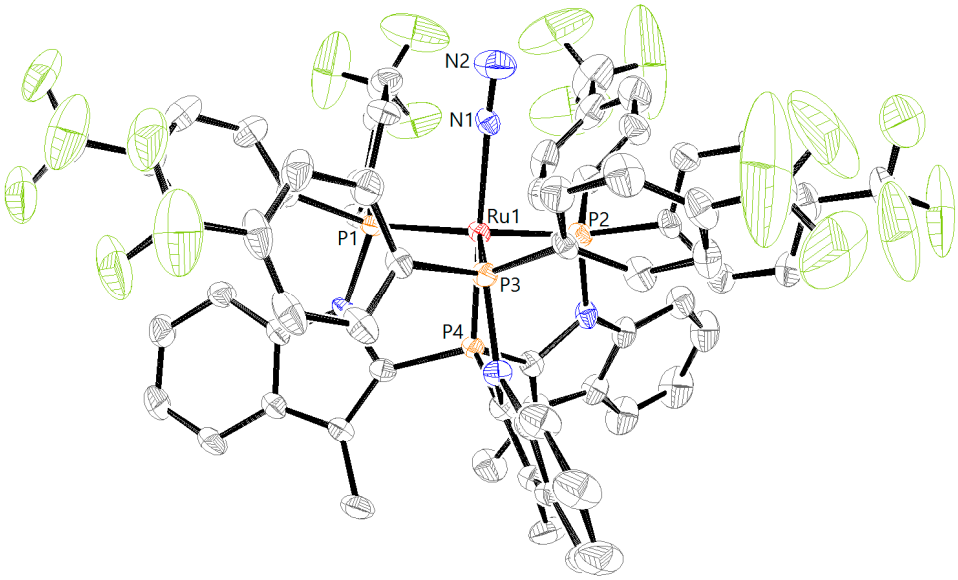

Figure 10. ORTEP drawing of $RuN_2\mathbf{L1^{CF3}}$ (top, CCDC 1574142) showing one of the two rotamers. Thermal ellipsoids are set at 50% probability. Solvent molecules and hydrogen atoms have been omitted for clarity.

The dinitrogen ligand in all of these ruthenium complexes is weakly coordinating as judged by the relatively small IR-shifts compared to that of free N_2 (ν = 2359 cm^{-1}) (Table 2). Preliminary experiments show no dinitrogen reduction to ammonia when complex $RuCl_2\mathbf{L1^H}$ was subjected to excess reductant (KC_8) in the presence of acid ($\{H(OEt_2)_2\}\{BArF_{24}\}$). Therefore, we set out to explore the reactivity of the tripodal tetraphosphine ruthenium(II) complexes for dinitrogen reduction with chlorosilanes (Figure 11), which follows a different mechanism [24].

$$N_2 + KC_8\ (100\ eq) + Me_3SiCl\ (100\ eq) \xrightarrow[THF,\ rt]{RuCl_2\mathbf{L}} (Me_3Si)_3N$$

Figure 11. Reduction of dinitrogen with KC_8, Me_3SiCl and $RuCl_2\mathbf{L}$ forming $(Me_3Si)_3N$.

A mixture of the $RuCl_2$**L** complexes with 100 equiv of KC_8 and 100 equiv of chlorotrimethylsilane in 10 mL THF at room temperature under an atmosphere of dinitrogen was stirred for 1 day, whereafter an aliquot of the reaction mixture was analyzed by GC. Modest yields of ~1.5 equivalents of $(Me_3Si)_3N$ relative to Ru were detected, regardless of the complex used (Table 3). The use of metallic sodium as reductant or longer reaction times did not increase the overall yield. In the absence of ruthenium only traces of $(Me_3Si)_3N$ could be detected.

Table 3. Formation of $(Me_3Si)_3N$ with $RuCl_2$**L** complexes.

Complex	Equiv $(Me_3Si)_3N$ [a]
$RuCl_2$**L1**^{CF3}	0.92 [b]
$RuCl_2$**L1**^{H}	1.83 [b]
$RuCl_2$**L1**^{OMe}	1.74 [b]
$RuCl_2$**L2**^{H}	1.40 [b]
$[Ru(\eta^6\text{-benzene})Cl(\mu\text{-}Cl)]_2$	1.29 [c]
-	trace

[a] Conditions: ~33 µmol of the complex was suspended together with KC_8 (100 equiv) in 10 mL THF whereafter the chlorotrimethylsilane (100 equiv) was added. The suspension was stirred for 23 h at room temperature; [b] Average of two runs; [c] Equivalents per ruthenium atom.

To gain more insight on the N_2 activation using these novel ruthenium complexes, the reduction was followed in time for complexes $RuCl_2$**L1**^{H} and $RuCl_2$**L2**^{H}, analyzing aliquots of the reaction mixture every hour. The reaction profile shows an incubation period of 1 h before product formation is observed (Figure 12). Such an incubation period was also reported for various other iron and cobalt systems that were investigated for N_2 reduction under comparable conditions [24–26], and which all showed similar activities for the formation of tris(trimethylsilyl)amine, regardless of the initial catalyst structure. It was speculated that the catalytically active species are generated after ligand dissociation from these iron and cobalt pre-catalysts. The exact nature of the reported catalysts could not be elucidated, as no dinitrogen-containing species were detected in these previous studies; however, test experiments pointed to a molecular nature of the catalyst [24,25].

Given that our complexes also show an incubation period and that electronic effects induced by ligand modification do not affect the catalytic activity, we speculate that our Ru-complexes are all pre-catalysts. To further test this hypothesis, we performed a catalytic reaction with $[Ru(\eta^6\text{-benzene})Cl(\mu\text{-}Cl)]_2$ in the absence of any tripodal indolyl-phosphine ligand under the same reaction conditions. Comparable amounts (1.29 equiv relative to Ru) of silylamine were formed in this control experiment, which indeed suggests ligand dissociation to activate the catalyst. Thus, these ligands cannot prevent metal leaching under the strongly reducing conditions used. Ex-situ ^{31}P NMR spectroscopy of the $RuCl_2$**L1**^{H} catalytic system showed the absence of the signals of the ruthenium complex pointing to decomposition of the pre-catalyst under the applied conditions.

Next, we investigated the potential of these Ru-species in the catalytic dehydrogenation of formic acid (Figure 13), given our interest in the reversible storage of H_2 into liquid fuels [27–33]. For Ru-catalysts, formic acid dehydrogenation is accelerated when more electron-rich ligands are employed, as was shown by Himeda et al., who used a series of bipyridine ligands with various substituents at the *para* position (–OH, –OMe, –Me, $–CO_2H$, and –H) [34]. With the various substituted tripodal tetraphosphine ligands **L1** and **L2** in hand, we anticipated to observe similar effects for the corresponding complexes in the formic acid dehydrogenation. The $RuCl_2$**L** complexes are coordinatively saturated, which necessitates chloride abstraction using $AgBF_4$ to allow for substrate activation. Addition of 1.2 mmol of formic acid under nitrogen to a refluxing solution of a mixture of Ru-precatalyst (8.5 µmol) and $AgBF_4$ (17 µmol) in 3 mL THF pre-activated for 2 h (initial concentration of formic acid: 0.4 M, substrate to catalyst ratio: 140) led to gas production within 1–5 min. The reactions were monitored volumetrically with a gas burette for one hour (see experimental section for a schematic representation). A typical time profile of the dehydrogenation reaction with catalyst $RuCl_2$**L1**^{OMe} is

displayed in Figure 14. The overall results of the different catalysts used in the dehydrogenation of formic acid are presented in Table 4. The gas outlet was analyzed using gas chromatography, which confirmed presence of both CO_2 and H_2, while no traces of CO were detected (detection limit of the GC for carbon monoxide was δ = 10 ppm). Under the described conditions, all the substrate is used within less than 2 h. Subsequent addition of aliquots of formic acid allowed for continuation of the reaction without an observed decrease in activity for at least 6 h.

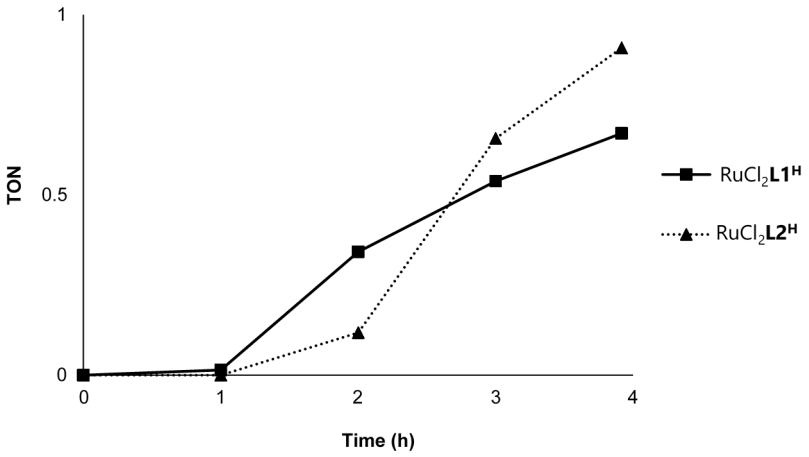

Figure 12. Dinitrogen reduction over a period of 4 h with catalysts $RuCl_2$**L1**$^{\mathbf{H}}$ and $RuCl_2$**L2**$^{\mathbf{H}}$. Turnover number (TON) is defined as equivalents of $(Me_3Si)_3N$ formed per ruthenium atom.

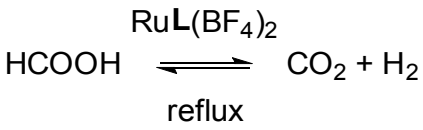

Figure 13. Formic acid decomposition by the Ru**L**$(BF_4)_2$ complexes.

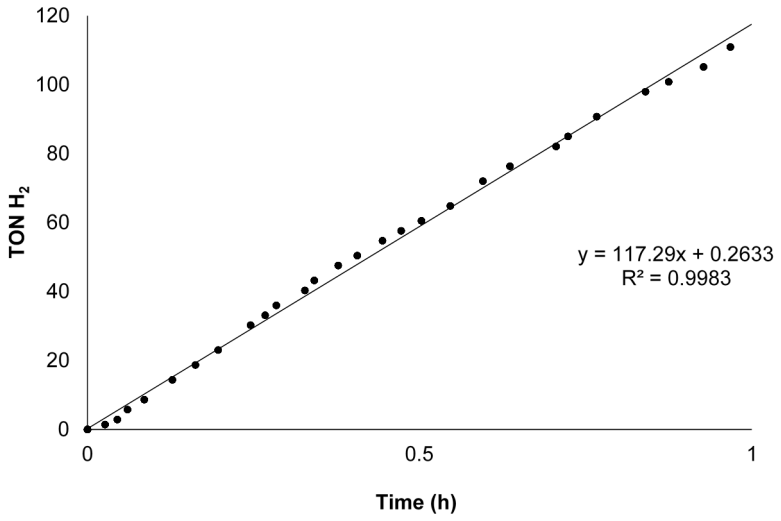

Figure 14. Hydrogen evolution from formic acid with catalyst $RuCl_2$**L1**$^{\mathbf{OMe}}$ as detected volumetrically with a gas burette. After 1 h, the burette contained 20 mL of H_2.

Table 4. Activities of $RuCl_2$**L** catalysts in the formic acid decomposition reaction.

Complex	TOF (h^{-1}) [a]
$RuCl_2$**L1**^{CF3}	124
$RuCl_2$**L1**^{H}	76
$RuCl_2$**L1**^{OMe}	121
$RuCl_2$**L2**^{H}	33
–	– [b]
[{$RuCl_2$(*p*-cymene)}$_2$]	1540 [c]

[a] Conditions: ~8.5 µmol preactivated catalyst (2 equiv $AgBF_4$ $RuCl_2$L. 2 h), 3 mL THF, 45 µL (1.2 mmol) HCOOH (catalyst to substrate ratio: 1:140), reflux temperature, 1 h reaction time, Turnover frequency (TOF, defined as number of equivalents of H_2 produced by the catalyst in one hour) is the average of two catalytic runs. The gas was collected volumetrically with a burette; [b] Conditions: 3 mL THF, 45 µL (1.2 mmol) HCOOH, reflux temperature, 30 min reaction time. [c] Conditions: ~6.5 µmol catalyst, 7 mmol ionic liquid, 17.6 mmol HCOOH (catalyst to substrate ratio: 1:2700), 80 °C, 7 h reaction time. Data taken from ref. [35].

Complexes $RuCl_2$**L1**^{OMe}, $RuCl_2$**L1**^{H}, and $RuCl_2$**L2**^{H} follow the same trend as noticed by Himeda [34], with the most electron-rich complex $RuCl_2$**L1**^{OMe} giving the highest activity (Turnover frequency (TOF) = 121 h^{-1}) followed by $RuCl_2$**L1**^{H} (TOF = 76 h^{-1}) and the least electron-rich $RuCl_2$**L2**^{H} (TOF = 33 h^{-1}). Interestingly, the $RuCl_2$**L1**^{CF3} complex (TOF = 124 h^{-1}) shows a comparable, even slightly higher activity to the electron-rich $RuCl_2$**L1**^{OMe} complex. The reason for this unusual observation is currently not clear. The TOFs found for the $RuCl_2$L complexes in the formic acid decomposition reaction are relatively low compared to reported systems based on Ir and Ru. For instance TOF of 487,500 h^{-1} was obtained with [Cp*Ir(L)Cl]Cl (L = 2,2′-bis-2-imidazoline) in neat HCOOH at 90 °C [36], TOF of 24,000 h^{-1} in boiling HCOOH/dioxane using [K(dme)$_2$][RuH(trop$_2$dad)] (trop$_2$dad = 1,4-bis(5H-dibenzo[a,d]cyclohepten-5-yl)-1,4-diazabuta-1,3-diene [37], TOF of 4556 h^{-1} with the more related Ru(H)$_2$(P4) complexes (P4 = *meso*-1,1,4,7,10,10-hexaphenyl-1,4,7,10-tetraphosphadecane) in HCOOH/*N*,*N*-dimethyloctylamine/propylene carbonate mixtures at 80 °C [38]. However, these initial results show that the $RuCl_2$**L** complexes are active in the dehydrogenation of formic acid and that the reactivity can be steered by ligand modification. Further reactivity studies with these complexes should be performed to elucidate the mechanism of the reaction and to find the maximum capacities (stability, temperature, solvent) of these catalysts.

3. Materials and Methods

All reactions were carried out under an atmosphere of nitrogen or argon using standard Schlenk techniques or in the glovebox. Reagents were purchased from commercial suppliers and used without further purification. THF, pentane, hexane, and Et_2O were distilled from sodium benzophenone ketyl. These solvents were degassed using the freeze–pump–thaw method (three cycles) and stored under dinitrogen atmosphere. CH_2Cl_2 was distilled from CaH_2 under dinitrogen. NMR spectra (^{1}H, ^{31}P, and ^{13}C{^{1}H, ^{31}P}) were measured on a Bruker DRX 500, Bruker AV 400, Bruker DRX 300, or on a Bruker AV 300 spectrometer (Bruker, Billerica, MA, USA). IR spectra (ATR mode) were recorded with a Bruker Alpha-p FT-IR spectrometer (Bruker, Billerica, MA, USA). High resolution mass spectra were recorded on a JEOL AccuTOF LC, JMS-T100LP mass spectrometer (JEOL, Tokyo, Japan) using cold electron-spray ionization (CSI) at −40 °C. GC measurements were performed on a Shimadzu GC-17A Gas Chromatograph (Shimadzu Corporation, Kyoto, Japan) with a Supelco SPB-1 fused silica capillary column. Tris-2-(3-methylindolyl)phosphine [14], **L1**^{H} [14], **L2**^{H} [14] and potassium graphite (KC_8) [39] were prepared according to literature procedures. Chlorobis[4-(trifluoromethyl)phenyl]phosphine (Alfa Aesar, Haverhill, MA, USA) and chlorobis[4-methoxyphenyl]phosphine (Sigma Aldrich, St. Louis, MO, USA) are commercially available chemicals and were used as received.

Tris-2-(3-methyl-*N*-di[4-(trifluoromethyl)phenyl]phosphinoindolyl)phosphine (L1^{CF3}) was prepared in the analogous way to **L1**^{H} using chlorobis[4-(trifluoromethyl)phenyl]phosphine:

To a solution of tris-2-(3-methylindolyl)phosphine (1.9 g, 4.53 mmol) in THF (50 mL) was added *n*-BuLi (2.5 M in hexanes, 5.7 mL, 14.3 mmol) at −78 °C. The resulting solution was stirred for 1 h and chlorobis[4-(trifluoromethyl)phenyl]phosphine (3.5 mL, 14.0 mmol) was added. The reaction mixture was stirred for 16 h and allowed to warm slowly to room temperature. The resulting suspension was concentrated in vacuo and dissolved in CH_2Cl_2 (total amount of 50 mL including washing of the pads). The suspension was filtered through a pad of basic alumina and subsequently through a pad of SiO_2. The solvent was removed under reduced pressure and resulted in a yellow foam. This yellow foam was purified by SiO_2 chromatography using a gradient from pure hexane to 2% Et_2O in hexane. Yield: 2.66 g (42%). ^{1}H NMR (300 MHz $CDCl_3$) δ: 7.44 (d, *J* = 8.6 Hz, 15H), 7.33–7.22 (m, 6H), 7.21–7.14 (m, 6H), 7.11 (t, *J* = 7.6 Hz, 3H), 6.93 (t, *J* = 7.8 Hz, 3H), 6.59 (d, *J* = 8.4 Hz, 3H), 2.14 (s, 9H). ^{19}F NMR (282 MHz, $CDCl_3$) δ = −60.78 ppm. ^{31}P NMR (121 MHz, $CDCl_3$) δ: 32.63 (d, *J* = 151.2 Hz, 3P), −76.09 (q, *J* = 151.6 Hz, 1P). ^{13}C NMR (75 MHz, $CDCl_3$) δ: 1140.28, 140.13, 139.77, 139.53, 139.36, 133.67, 131.91, 131.71, 131.62, 131.43, 129.27, 125.60, 125.53, 125.42, 125.33, 123.72, 122.00, 121.21, 119.50, 113.97, 9.94 ppm.

Tris-2-(3-methyl-*N*-di[4-methoxyphenyl]phosphinoindolyl)phosphine ($L1^{OMe}$) was prepared in the analogous way to $\mathbf{L1^H}$ using chlorobis[4-methoxyphenyl]phosphine: To a solution of tris-2-(3-methylindolyl)phosphine (2.20 g, 5.22 mmol) in THF (50 mL) was added *n*-BuLi (2.5 M in hexanes, 6.6mL, 16.44 mmol) at −78 °C. The resulting solution was stirred for 1 h and chlorobis[4-methoxyphenyl]phosphine (4.83 g, 17.23 mmol) dissolved in 10 mL THF was added. The reaction mixture was stirred for 3 days and allowed to warm to room temperature. The resulting suspension was concentrated in vacuo, dissolved in CH_2Cl_2 (total amount of 50 mL including washing of the pads) and filtered through a pad of basic alumina. Evaporation of the solvent and trituration with Et_2O yielded a white solid which was recrystallized from vapor diffusion evaporation of Et_2O to a concentrated THF solution. Washing with Et_2O and drying under vacuum yielded the ligand in pure form. Yield: 4.03 g (67%). ^{1}H NMR (300 MHz, $(CD_3)_2CO$): δ 7.46 (d, *J* = 7.9, 1.0 Hz, 3H), 7.39–7.27 (m, 6H), 7.20–7.07 (m, 6H), 7.05–6.95 (t, 3H), 6.94–6.81 (m, 12H), 6.77 (d, 6H), 3.74 (s, 18H), 2.01 (s, 9H) ppm. ^{31}P NMR (122 MHz, $(CD_3)_2CO$): δ 36.83 (d, *J* = 166.0 Hz, 3P), −76.21 (q, *J* = 166.7, 1P) ppm. ^{13}C NMR (75 MHz, $(CD_3)_2CO$) δ: 161.42, 141.33, 141.16, 134.63, 134.33, 134.06, 134.03, 127.95, 127.78, 127.58, 127.38, 124.22, 123.07, 120.83, 119.56, 115.06, 114.91, 114.86, 114.81, 114.77, 55.52, 9.87 ppm.

$RuCl_2L1^{CF3}$: **$L1^{CF3}$** (1.3732 g, 0.99 mmol) and [Ru(η^6-benzene)Cl(μCl)]$_2$ (249.3 mg, 0.50 mmol) were suspended in THF (4 mL) and toluene (8 mL) and stirred at 60 °C for 64 h. After cooling, the yellow precipitated complex was filtered, washed with toluene (1 × 2 mL) and pentane (3 × 3 mL), and dried overnight in the vacuum oven at 40 °C. Yield: 0.9914 g (64%) of a yellow solid. Recrystallization of the complex by layering a DCM solution with pentane at 5 °C gave crystals suitable for X-ray diffraction analysis. ^{1}H NMR (300 MHz, $CDCl_3$): δ 7.72 (dd, *J* = 10.8, 8.0 Hz, 3H), 7.59 (dt, *J* = 10.5, 5.3 Hz, 4H), 7.53–7.31 (m, 8H), 7.24 (t, *J* = 7.6 Hz, 4H), 7.18–7.01 (m, 7H), 6.99–6.81 (m, 7H), 6.11 (d, *J* = 8.5 Hz, 2H), 5.86 (d, *J* = 8.5 Hz, 1H), 2.93 (s, 6H), 2.69 (s, 3H) ppm. ^{31}P NMR (122 MHz, $CDCl_3$): δ 99.83 (dt, *J* = 31.5, 26.4 Hz, 1P), 78.90 (t, *J* = 26.3 Hz, 2P), 49.00 (dt, *J* = 30.3, 26.7 Hz, 1P) ppm. ^{13}C NMR (75 MHz, $CDCl_3$): δ 134.83, 134.73, 133.95, 133.82, 132.74, 132.63, 132.31, 132.18, 131.43, 131.31, 129.54, 128.96, 128.73, 128.49, 128.18, 128.05, 127.88, 127.74, 127.68, 127.58, 127.44, 126.91, 126.76, 126.44, 126.30, 125.15, 124.71, 124.64, 122.90, 122.45, 122.32, 120.76, 120.22, 117.80, 115.44, 115.00, 13.64, 12.27, 11.99. ppm. Mass Analysis (CSI) $[C_{69}H_{45}Cl_1F_{18}N_3P_4Ru]^+$: calc: 1518.1024 found 1518.1067.

$RuCl_2L1^{OMe}$: **$L1^{OMe}$** (1.02 g, 0.88 mmol) and [Ru(η^6-benzene)Cl(μCl)]$_2$ (227.9 mg, 0.45 mmol) were suspended in THF (4 mL) and toluene (8 mL) and stirred at 120 °C for 3 days leaving a pale brown solution. Upon cooling of the reaction mixture, an off-white solid precipitated. This solid was filtered and washed with hexane (3 × 3 mL) and dried overnight in the vacuum oven at 40 °C, resulting in the product as a brown-white solid. Yield: 1.15 g of an off-white solid (97.8%). ^{1}H NMR (300 MHz, $CDCl_3$): δ 7.66 (d, *J* = 8.0 Hz, 2H), 7.58 (d, *J* = 7.9 Hz, 1H), 7.44–7.32 (m, 4H), 7.32–7.24 (m, 1H), 7.24–7.02 (m, 10H), 6.89 (q, *J* = 7.8, 6.9 Hz, 4H), 6.77 (t, *J* = 7.8 Hz, 1H), 6.68 (d, *J* = 8.5 Hz, 4H),

6.28 (d, *J* = 8.5 Hz, 2H), 6.24 (d, *J* = 7.9 Hz, 2H), 6.12 (d, *J* = 8.5 Hz, 4H), 5.90 (d, *J* = 8.5 Hz, 1H), 3.70 (d, *J* = 1.8 Hz, 12H), 3.62 (s, 6H), 2.84 (s, 6H), 2.60 (s, 3H) ppm. ^{31}P NMR (121 MHz, $CDCl_3$): δ 107.24 (dt, *J* = 32.0, 26.0 Hz, 1P), 83.78 (t, *J* = 26.6 Hz, 2P), 54.51 (dt, *J* = 30.9, 26.9 Hz, 1P) ppm. ^{13}C{^{1}H,^{31}P} NMR (75 MHz, $CDCl_3$): δ = 159.95, 159.46, 139.85, 139.70, 135.39, 135.35, 135.27, 133.02, 132.98, 132.86, 123.72, 123.69, 121.47, 121.27, 120.20, 117.09, 113.38, 113.29, 112.88, 112.72, 112.03, 111.96, 111.89, 77.43, 77.00, 76.58, 54.90, 54.82, 54.79, 11.92, 11.68 ppm. Mass Analysis (CSI) $[C_{69}H_{63}ClN_3O_6P_4Ru]^+$: calc: 1290.2399 found: 1290.2400.

$RuCl_2L2^H$: **$L2^H$** (587.3 mg, 0.60 mmol) and [Ru(η^6-benzene)Cl(μ-Cl)]$_2$ (150.1 mg, 0.30 mmol) were suspended in THF (3 mL) and toluene (6 mL) and stirred at 120 °C for 64 h. After cooling, 20 mL of hexane was added, which resulted in the precipitation of a yellow solid. The solid was filtered, washed with hexane (3 × 3 mL), and dried overnight in the vacuum oven at 60 °C. Yield: 477.5 mg (69.1%) of a yellow solid. Recrystallization of the complex by layering a DCM solution with pentane at 5 °C gave crystals suitable for X-ray diffraction analysis. ^{1}H NMR (300 MHz, $CDCl_3$): δ 7.90 (dd, *J* = 11.6, 7.7 Hz, 2H), 7.84–7.65 (m, 6H), 7.60 (d, *J* = 7.8 Hz, 1H), 7.53 (t, *J* = 9.3 Hz, 3H), 7.45 (d, *J* = 7.8 Hz, 1H), 7.37 (t, *J* = 7.6 Hz, 1H), 7.32–7.12 (m, 9H), 7.11–6.92 (m, 6H), 6.90–6.75 (m, 7H), 6.70 (d, *J* = 8.4 Hz, 1H), 6.36 (t, *J* = 8.4 Hz, 3H), 6.23 (dd, *J* = 7.5 Hz, 2H), 1.97 (s, 3H), 1.72 (s, 3H), 1.40 (s, 3H) ppm. ^{31}P NMR (121 MHz, $CDCl_3$): δ 144.43 (dt, *J* = 38.9, 37.8 Hz, 1P), 39.22 (dt, *J* = 45.0, 23.6 Hz, 1P), 24.70 (ddd, *J* = 328.6, 31.0, 21.1 Hz, 1P), 16.62 (ddd, *J* = 331.4, 39.7, 25.6 Hz, 1P) ppm. ^{13}C NMR (75 MHz, $CDCl_3$): δ 134.83, 134.73, 133.95, 133.82, 132.74, 132.63, 132.31, 132.18, 131.43, 131.31, 129.54, 128.73, 128.49, 128.18, 128.05, 127.88, 127.74, 127.68, 127.58, 127.44, 126.91, 126.76, 126.44, 126.31, 125.15, 124.71, 124.64, 122.90, 122.45, 122.32, 120.76, 120.22, 117.80, 115.44, 115.00, 13.64, 12.27, 11.99 ppm. Mass Analysis (CSI) $[C_{63}H_{51}ClN_3P_4Ru]^+$: calc: 1110.1789; found: 1110.1779.

*3.1. Reduction of $RuCl_2$**L** to RuN_2**L***

$RuCl_2$**L** (±17 μmol) and KC_8 (2–3 equiv) were transferred to a flame-dried Schlenk flask in the glovebox. THF (2 mL) was added and the suspension was stirred for two to three hours; after filtration, a red solution was obtained. Part of this solution was used for in-situ infrared spectrometry, part of the solution was used for in-situ ^{31}P NMR analysis, and the rest of the solution was set for crystallization via slow diffusion evaporation of pentane. Applying this procedure to $RuCl_2$**$L1^{OMe}$** led to formation of a purple solution after filtration, which did not show an infrared band after two hours. However, after one day, the solution turned more red and the corresponding infrared band could be detected. The infrared analysis of the thus obtained solutions yielded the corresponding infrared bands as given in Table 2. The ^{31}P-NMR analysis showed the presence of one doublet and one quartet, indicative of a symmetric species, which corresponds with the proposed trigonal bipyramidal geometry.

3.2. Catalysis: Dinitrogen Reduction

The catalyst (33 μmol) and KC_8 (100 equiv) were transferred to a 100 mL flame-dried Schlenk flask equipped with a glass stirring bar in the glovebox. 10 mL of dry THF was added, followed by the addition of the chlorotrimethylsilane (100 equiv). The suspension was stirred overnight. A quantity of 10 μL of *n*-decane was added as internal standard, whereafter a filtered aliquot of the reaction mixture was measured on the Gas-GC.

3.3. Catalysis in Time: Dinitrogen Reduction

The same procedure as for the normal nitrogen reduction was used, adding the 10 μL of *n*-decane right away and taking a filtered aliquot of the reaction mixture every hour, which was subsequently measured on the Gas-GC.

3.4. Catalysis: Formic Acid Dehydrogenation

Hydrogen evolution was initiated by the addition of formic acid (45 μL, 1.2 mmol) to a solution of catalyst (±8.5 μmol) in refluxing THF (3 mL) in a 10 mL reaction flask equipped with a condenser.

The gas was cooled via a condenser, with the outlet connected to a burette filled with water (Figure 15). The displacement of the water level in the burette was measured in time. The second burette was also filled with water and used to compensate for pressure buildup, keeping the water levels at equal height. The results are shown in Table 5.

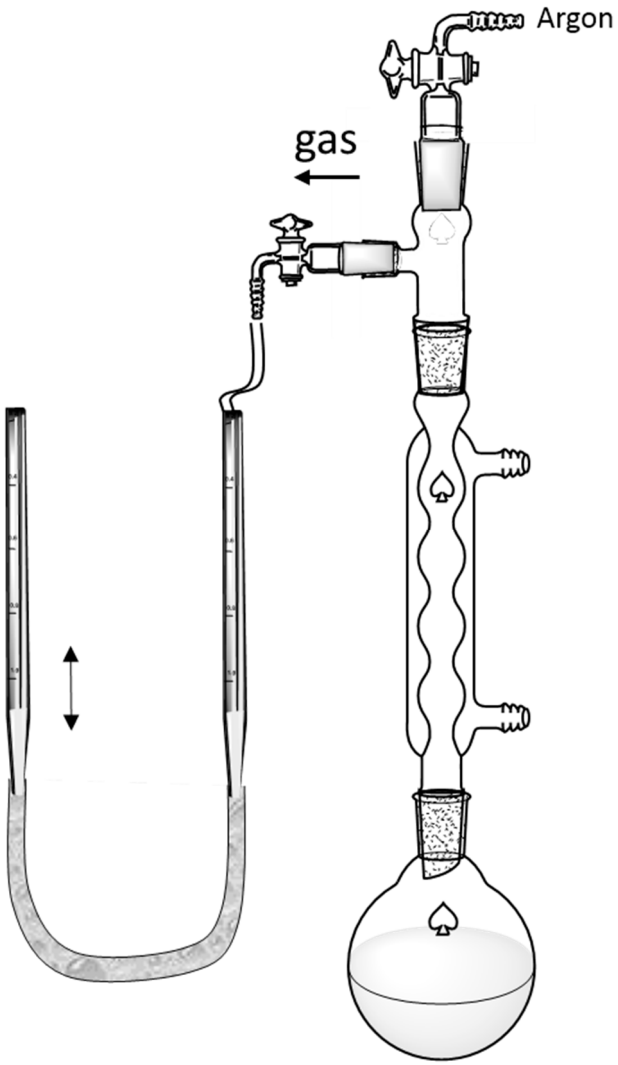

Figure 15. Hydrogen evolution set up.

Table 5. Duplo measurements for formic acid dehydrogenation by the depicted catalysts.

Complex	TOF (h^{-1}) #1	TOF (h^{-1}) #2	TOF (h^{-1}) Average
$RuCl_2$**L1**^{CF3}	120.8	127.2	124
$RuCl_2$**L1**^{H}	79.3	71.9	75.6
$RuCl_2$**L1**^{OMe}	123.5	117.4	120.5
$RuCl_2$**L2**^{H}	22.4	42.7	32.6

TOF_{H2} was calculated using Equation (1) [40].

$$TOF_{H2} = \frac{V_{obs} \cdot 0.5}{V_m \cdot n_{cat}} \quad (1)$$

V_{obs}: measured gas volume displacement cylinder [mL]; V_m: molar gas volume: 24.49 [mL/mmol]; n_{cat}: amount of catalyst [mmol].

3.5. X-ray Diffraction Analysis

Crystallographic data was obtained using a Bruker D8 Quest Eco diffractometer equipped with a Triumph monochromator. The intensities were integrated with the SAINT software package [41]. Multiscan absorption correction and scaling was performed with *SADABS* [42]. The structure was solved with Intrinsic Phasing Methods using *SHELXT* [43]. Least-squares refinement was performed with *SHELXL* 2013 [44] against F^2 of all reflections. Non-hydrogen atoms were refined freely with anisotropic displacement parameters. All hydrogen atoms were located in difference Fourier maps and refined with a riding model. All structures have solvent-accessible voids filled with disordered solvent. Their contribution to the structure factors in the refinement was taken into account with the PLATON/SQUEEZE approach [45] (Table 6).

Table 6. Crystallographic data for $RuCl_2$**L1**^{CF3}, $RuCl_2$**L2**^{H} and RuN_2**L1**^{H}.

Complex	$RuCl_2$**L1**^{CF3}	$RuCl_2$**L2**^{H}	RuN_2**L1**^{CF3}
Empirical formula	$C_{69}H_{45}Cl_2F_{18}N_3P_4Ru$ + solvent	$C_{63}H_{51}Cl_2N_3P_4Ru$, $2(CH_2Cl_2)$ + solvent	$C_{69}H_{45}F_{18}N_5P_4Ru$ + solvent
FW	1553.93 [a]	1315.77 [a]	1511.05 [a]
Temperature [K]	150	150	150
Radiation	Mo Kα	Mo Kα	Mo Kα
Wavelength [Å]	0.71073	0.71073	0.71073
Cryst syst.	monoclinic	monoclinic	monoclinic
Space group	*C* 2/*c*	*P* 21/*n*	P 21/*c*
a [Å]	21.594(3)	19.1879(9)	14.2851(6)
b [Å]	27.753(4)	18.1604(8)	18.9090(8)
c [Å]	23.938(3)	19.7879(9)	29.8721(12)
α [deg.]	90	90	90
β [deg.]	93.631(3)	91.012(2)	97.011(2)
γ [deg.]	90	90	90
Volume [Å^3]	14317(3)	6894.2(5)	8008.6(6)
Z	8	4	4
Color	pale yellow	yellow	dark red
θ-max	25.135	25.030	26.450
Density [kg·m^{-3}]	1.442 [a]	1.268 [a]	1.253 [a]
Absorp. Coeff. [mm^{-1}]	0.472 [a]	0.591 [a]	0.356 [a]
F(000)	6240 [a]	2688.0	3040 [a]
$R_1/wR_2/S$	0.0715/0.1975/1.053	0.0412/0.1435/1.134	0.0666/0.2002/1.436

[a] Excluding the disordered solvent contribution.

$RuCl_2$**L1**^{CF3}: The structure contains voids (2544 Å^3 per unit cell) filled with disordered solvent molecules. Their contribution to the structure factors was secured by back-Fourier transformation using the SQUEEZE routine of the PLATON package [45], resulting in 671 electrons per unit cell which corresponds to 16 disordered molecules of CH_2Cl_2 per unit cell. Alerts A and most Alerts B generated by the IUCr checkCIF program resulted from large displacement parameters of F atoms implying intense rotation of the CF_3 groups of the **L1**^{CF3} ligand. Thirteen FCF reflections below θ-min were obscured by the beam-stop which generated Alert B.

$RuCl_2$**L2**^{H}: The structure contains voids (1518 Å^3 per unit cell) filled with disordered solvent molecules. Their contribution to the structure factors was secured by back-Fourier transformation using the SQUEEZE routine of the PLATON package [45], resulting in 503 electrons per unit cell which corresponds to 12 disordered molecules of CH_2Cl_2 per unit cell. Eleven FCF reflections below θ-min were obscured by the beam-stop which generated Alert B by the IUCr checkCIF program.

RuN_2**L1**^{CF3}: The structure contains voids (2224 Å^3 per unit cell) filled with disordered solvent molecules. Their contribution to the structure factors was secured by back-Fourier transformation using the SQUEEZE routine of the PLATON package [45], resulting in 514 electrons per unit cell which corresponds to 12 disordered molecules of pentane per unit cell. Alerts A generated by the IUCr checkCIF program resulted from large displacement parameters of F atoms implying intense rotation of the CF_3 groups of the **L1**^{CF3} ligand. Thirteen FCF reflections below θ-min were obscured by the beam-stop which generated Alert B.

CCDC 1574140, 1574141, 1574142 contains the supplementary crystallographic data for this paper. These data can be obtained free of charge via http://www.ccdc.cam.ac.uk/conts/retrieving.

html (or from the CCDC, 12 Union Road, Cambridge CB2 1EZ, UK; Fax: +44-1223-336033; E-mail: deposit@ccdc.cam.ac.uk).

4. Conclusions

In conclusion, we have shown the formation of new ruthenium complexes based on a tripodal 3-methylindolephosphine scaffold. The ligand has two structural ("linkage") isomers, and, for one of those isomers, several analogues with electron-withdrawing and -donating groups were prepared. These ligands were successfully coordinated to $[Ru(\eta^6\text{-benzene})Cl(\mu\text{-}Cl)]_2$, resulting in the formation of octahedral complexes with the two chlorides in *cis* position. The stoichiometric reduction of these complexes with KC_8 yielded the corresponding dinitrogen complexes. Electronic effects in the ligands translated to a change in the N≡N stretch frequency of the coordinated dinitrogen. The complexes were studied in the N_2 reduction with chlorosilanes and KC_8, yielding stoichiometric amounts of the silylamines. When the reaction was followed in time, an incubation period was observed. This incubation period, and the near-identical activities found for all complexes tested, suggests that these species are mere pre-catalysts. The complexes were also employed for formic acid dehydrogenation. Turnover frequencies between 33 and 124 h^{-1} were reached, depending on the ligand used, clearly showing that the electronic properties of the ligand do have an effect in this reaction. Further studies with these complexes have to be performed to elucidate the reaction mechanism and stability of the catalysts.

Supplementary Materials: The following are available online at www.mdpi.com/2304-6740/5/4/73/s1, Figures S1–S4, cif and cif-checked files.

Acknowledgments: We thank the National Research School Combination Catalysis (NRSC-C) and the Netherlands Organization for Scientific Research (NWO-CW, VENI grant 722.013.002 for W.I.D.) and the University of Amsterdam (RPA Sustainable Chemistry) for funding. We thank Jan-Meine Ernsting for assistance with NMR spectroscopy and Ed Zuidinga for mass spectrometry measurements.

Author Contributions: Fenna F. van de Watering, Wojciech I. Dzik, Bas de Bruin and Joost N. H. Reek conceived and designed the experiments; Fenna F. van de Watering performed the experiments; Nicol Heijtbrink performed control experiments; Fenna F. van de Watering, Bas de Bruin, Jarl Ivar van der Vlugt and Wojciech I. Dzik analyzed the data; Fenna F. van de Watering, Jarl Ivar van der Vlugt, Wojciech I. Dzik, Bas de Bruin and Joost N. H. Reek wrote the paper.

Conflicts of Interest: The authors declare no conflict of interest.

References

1. Field, L.D.; Messerle, B.A.; Smernik, R.J. Synthesis and Properties of Iron(II) Hydride Complexes Containing the Tripodal Tetraphosphine Ligand $P(CH_2CH_2PMe_2)_3$. *Inorg. Chem.* **1997**, *36*, 5984–5990. [CrossRef] [PubMed]
2. Bruneau, C.; Dixneuf, P.H. *Ruthenium in Catalysis*; Bruneau, C., Dixneuf, P.H., Eds.; Springer: Rennes, France, 2014; Volume 48.
3. Bianchini, C. Stoichiometric and catalytic functionalization reactions of alkynes at transition metal complexes stabilized by tripodal polyphosphine ligands. *Pure Appl. Chem.* **1991**, *63*, 829–834. [CrossRef]
4. Yandulov, D.V.; Schrock, R.R.; Rheingold, A.L.; Ceccarelli, C.; Davis, W.M. Synthesis and Reactions of Molybdenum Triamidoamine Complexes Containing Hexaisopropylterphenyl Substituents. *Inorg. Chem.* **2003**, *42*, 796–813. [CrossRef] [PubMed]
5. Mankad, N.P.; Whited, M.T.; Peters, J.C. Terminal Fe^{I}–N_2 and $Fe^{II}\cdots$H–C Interactions Supported by Tris(phosphino)silyl Ligands. *Angew. Chem. Int. Ed.* **2007**, *46*, 5768–5771. [CrossRef] [PubMed]
6. Moret, M.E.; Peters, J.C. Terminal Iron Dinitrogen and Iron Imide Complexes Supported by a Tris(phosphino)borane Ligand. *Angew. Chem. Int. Ed.* **2011**, *50*, 2063–2067. [CrossRef] [PubMed]
7. Creutz, S.E.; Peters, J.C. Catalytic Reduction of N_2 to NH_3 by an Fe–N_2 Complex Featuring a C–Atom Anchor. *J. Am. Chem. Soc.* **2014**, *136*, 1105–1115. [CrossRef] [PubMed]

8. Siedschlag, R.B.; Bernales, V.; Vogiatzis, K.D.; Planas, N.; Clouston, L.J.; Bill, E.; Gagliardi, L.; Lu, C.C. Catalytic Silylation of Dinitrogen with a Dicobalt Complex. *J. Am. Chem. Soc.* **2015**, *137*, 4638–4641. [CrossRef] [PubMed]
9. Del Castillo, T.J.; Thompson, N.B.; Peters, J.C. A Synthetic Single-Site Fe Nitrogenase: High Turnover, Freeze-Quench ^{57}Fe Mössbauer Data, and a Hydride Resting State. *J. Am. Chem. Soc.* **2016**, *138*, 5341–5350. [CrossRef] [PubMed]
10. Yandulov, D.V.; Schrock, R.R. Catalytic reduction of dinitrogen to ammonia at a single molybdenum center. *Science* **2003**, *301*, 76–78. [CrossRef] [PubMed]
11. Li, Y.-N.; Ma, R.; He, L.-N.; Diao, Z.-F. Homogeneous hydrogenation of carbon dioxide to methanol. *Catal. Sci. Technol.* **2014**, *4*, 1498–1512. [CrossRef]
12. Wang, W.H.; Himeda, Y.; Muckerman, J.T.; Manbeck, G.F.; Fujita, E. CO_2 Hydrogenation to Formate and Methanol as an Alternative to Photo- and Electrochemical CO_2 Reduction. *Chem. Rev.* **2015**, *115*, 12936–12973. [CrossRef] [PubMed]
13. Federsel, C.; Jackstell, R.; Boddien, A.; Laurenczy, G.; Beller, M. Ruthenium-Catalyzed Hydrogenation of Bicarbonate in Water. *ChemSusChem* **2010**, *3*, 1048–1050. [CrossRef] [PubMed]
14. Wassenaar, J.; de Bruin, B.; Siegler, M.A.; Spek, A.L.; Reek, J.N.H.; van der Vlugt, J.I. Activation of H_2 by a highly distorted Rh^{II} complex with a new C_3-symmetric tripodal tetraphosphine ligand. *Chem. Commun.* **2010**, *46*, 1232–1234. [CrossRef] [PubMed]
15. Wassenaar, J.; Siegler, M.A.; Spek, A.L.; De Bruin, B.; Reek, J.N.H.; van der Vlugt, J.I. Versatile New C_3-Symmetric Tripodal Tetraphosphine Ligands; Structural Flexibility to Stabilize Cu^{I} and Rh^{I} Species and Tune Their Reactivity. *Inorg. Chem.* **2010**, *49*, 6495–6508. [CrossRef] [PubMed]
16. van de Watering, F.F.; van der Vlugt, J.I.; Dzik, W.I.; de Bruin, B.; Reek, J.N.H. Metalloradical Reactivity of Ru^{I} and Ru^{0} Stabilized by an Indole-Based Tripodal Tetraphosphine Ligand. *Chem. Eur. J.* **2017**, *23*, 12709–12713. [CrossRef] [PubMed]
17. Yu, J.O.; Browning, C.S.; Farrar, D.H. Tris-2-(3-methylindolyl)phosphine as an anion receptor. *Chem. Commun.* **2008**, 1020–1022. [CrossRef] [PubMed]
18. Yu, J.O.; Lam, E.; Sereda, J.L.; Rampersad, N.C.; Lough, A.J.; Browning, C.S.; Farrar, D.H. 2-Indolylphosphines, a New Class of Tunable Ligands: Their Synthesis, Facile Derivatization, and Coordination to Palladium(II). *Organometallics* **2005**, *24*, 37–47. [CrossRef]
19. Yu, J.O. An Exploration of the Structural, Electronic, and Anion Binding Properties of 2-Indolylphosphines. Ph.D. Thesis, University of Toronto, Toronto, ON, Canada, 2008.
20. Ciclosi, M.; Lloret, J.; Estevan, F.; Lahuerta, P.; Sanaú, M.; Pérez-Prieto, J. A C_3-Symmetric Palladium Catalyst with a Phosphorus-Based Tripodal Ligand. *Angew. Chem. Int. Ed.* **2006**, *45*, 6741–6744. [CrossRef] [PubMed]
21. Ciclosi, M.; Estevan, F.; Lahuerta, P.; Passarelli, V.; Perez-Prieto, J.; Sanaú, M. Synthesis and reactivity of the novel hydride derivative $RhHCl(TIMP_3)$ ($HTIMP_3$ = tris[1-(diphenylphosphino)-3-methyl-1*H*-indol-2-yl]methane). *Dalton Trans.* **2009**, 2290–2297. [CrossRef] [PubMed]
22. Penno, D.; Koshevoy, I.O.; Estevan, F.; Sanaú, M.; Ubeda, M.A.; Pérez-Prieto, J. Synthesis of a New C_3-Symmetric Tripodal P4-Tetradentate Ligand and Its Application to the Formation of Chiral Metal Complexes. *Organometallics* **2010**, *29*, 703–706. [CrossRef]
23. Kuo, YY.; Haddow, M.F.; Jamieson, A.L.; Owen, G.R. Synthesis, structural characterisation and catalytic application of dichloro(η^6-*p*-cymene){diphenyl(3-methyl-2-indolyl)phosphine}-ruthenium(II) in the transfer hydrogenation of ketones. *Transit. Met. Chem.* **2013**, *38*, 641–648. [CrossRef]
24. Imayoshi, R.; Tanaka, H.; Matsuo, Y.; Yuki, M.; Nakajima, K.; Yoshizawa, K.; Nishibayashi, Y. Cobalt-Catalyzed Transformation of Molecular Dinitrogen into Silylamine under Ambient Reaction Conditions. *Chem. Eur. J.* **2015**, *21*, 8905–8909. [CrossRef] [PubMed]
25. Yuki, M.; Tanaka, H.; Sasaki, K.; Miyake, Y.; Yoshizawa, K.; Nishibayashi, Y. Iron-catalysed transformation of molecular dinitrogen into silylamine under ambient conditions. *Nat. Commun.* **2012**, *3*, 1254. [CrossRef] [PubMed]
26. Dzik, W.I. Silylation of Dinitrogen Catalyzed by Hydridodinitrogentris(Triphenylphosphine)Cobalt(I). *Inorganics* **2016**, *4*, 21. [CrossRef]
27. Oldenhof, S.; de Bruin, B.; Lutz, M.; Siegler, M.A.; Patureau, F.W.; van der Vlugt, J.I.; Reek, J.N.H. Base-Free Production of H_2 by Dehydrogenation of Formic Acid Using an Iridium–bisMETAMORPhos Complex. *Chem. Eur. J.* **2013**, *19*, 11507–11511. [CrossRef] [PubMed]

28. Oldenhof, S.; Lutz, M.; de Bruin, B.; van der Vlugt, J.I.; Reek, J.N.H. Dehydrogenation of formic acid by Ir–bisMETAMORPhos complexes: Experimental and computational insight into the role of a cooperative ligand. *Chem. Sci.* **2015**, *6*, 1027–1034. [CrossRef]
29. Oldenhof, S.; van der Vlugt, J.I.; Reek, J.N.H. Hydrogenation of CO_2 to formic acid with iridium^{III}(bisMETAMORPhos)(hydride): The role of a dormant *fac*-Ir^{III}(trihydride) and an active *trans*-Ir^{III}(dihydride) species. *Catal. Sci. Technol.* **2016**, *6*, 404–408. [CrossRef]
30. Jongbloed, L.S.; de Bruin, B.; Reek, J.N.H.; Lutz, M.; van der Vlugt, J.I. Reversible cyclometalation at Rh^{I} as a motif for metal–ligand bifunctional bond activation and base-free formic acid dehydrogenation. *Catal. Sci. Technol.* **2016**, *6*, 1320–1327. [CrossRef]
31. Van de Watering, F.F.; Lutz, M.; Dzik, W.I.; de Bruin, B.; Reek, J.N.H. Reactivity of a Ruthenium–Carbonyl Complex in the Methanol Dehydrogenation Reaction. *ChemCatChem* **2016**, *8*, 2752–2756. [CrossRef] [PubMed]
32. De Boer, S.Y.; Korstanje, T.J.; La Rooij, S.R.; Kox, R.; Reek, J.N.H.; van der Vlugt, J.I. Ruthenium PNN(O) Complexes: Cooperative Reactivity and Application as Catalysts for Acceptorless Dehydrogenative Coupling Reactions. *Organometallics* **2017**, *36*, 1541–1549. [CrossRef]
33. Trincado, M.; Sinha, V.; Rodriguez-Lugo, R.E.; Pribanic, B.; de Bruin, B.; Grützmacher, H. Homogeneously catalysed conversion of aqueous formaldehyde to H_2 and carbonate. *Nat. Commun.* **2017**, *8*, 14990. [CrossRef] [PubMed]
34. Himeda, Y.; Miyazawa, S.; Hirose, T. Interconversion between formic acid and H_2/CO_2 using rhodium and ruthenium catalysts for CO_2 fixation and H_2 storage. *ChemSusChem* **2011**, *4*, 487–493. [CrossRef] [PubMed]
35. Scholten, J.D.; Prechtl, M.H.G.; Dupont, J. Decomposition of Formic Acid Catalyzed by a Phosphine-Free Ruthenium Complex in a Task-Specific Ionic Liquid. *ChemCatChem* **2010**, *2*, 1265–1270. [CrossRef]
36. Wang, Z.; Lu, S.-M.; Li, J.; Wang, J.; Li, C. Unprecedentedly High Formic Acid Dehydrogenation Activity on an Iridium Complex with an *N*,*N*′-Diimine Ligand in Water. *Chem. Eur. J.* **2015**, *21*, 12592–12595. [CrossRef] [PubMed]
37. Rodríguez-Lugo, R.E.; Trincado, M.; Vogt, M.; Tewes, F.; Santiso-Quinones, G.; Grützmacher, H. A homogeneous transition metal complex for clean hydrogen production from methanol-water mixtures. *Nat. Chem.* **2013**, *5*, 342–347. [CrossRef] [PubMed]
38. Mellone, I.; Bertini, F.; Peruzzini, M.; Gonsalvi, L. An active, stable and recyclable Ru(II) tetraphosphine-based catalytic system for hydrogen production by selective formic acid dehydrogenation. *Catal. Sci. Technol.* **2016**, *6*, 6504–6512. [CrossRef]
39. Weitz, I.S.; Rabinovitz, M. The application of C_8K for organic synthesis: Reduction of substituted naphthalenes. *J. Chem. Soc. Perkin Trans.* **1993**, *1*, 117–120. [CrossRef]
40. Nielsen, M.; Alberico, E.; Baumann, W.; Drexler, H.-J.; Junge, H.; Gladiali, S.; Beller, M. Catalysis: A step closer to a methanol economy. *Nature* **2013**, *495*, 85–89. [CrossRef] [PubMed]
41. Bruker. *SAINT-Plus*; Bruker AXS Inc.: Madison, WI, USA, 2001.
42. Sheldrick, G.M. *SADABS and TWINABS*; Universität Göttingen: Göttingen, Germany, 2008.
43. Sheldrick, G.M. *SHELXT*; Universität Göttingen: Göttingen, Germany, 2012.
44. Sheldrick, G.M. *SHELXT*—Integrated space-group and crystal-structure determination. *Acta Cryst.* **2015**, *A71*, 3–8. [CrossRef] [PubMed]
45. Spek, A.L. Structure validation in chemical crystallography. *Acta Cryst.* **2009**, *D65*, 148–155. [CrossRef] [PubMed]